

# BiVO<sub>4</sub> thin film photoanodes grown by chemical vapor deposition†

Cite this: *Phys. Chem. Chem. Phys.*, 2014, 16, 1651

Esther Alarcón-Lladó,<sup>‡abc</sup> Le Chen,<sup>‡ac</sup> Mark Hettick,<sup>acd</sup> Neeka Mashouf,<sup>a</sup> Yongjing Lin,<sup>acd</sup> Ali Javey<sup>acd</sup> and Joel W. Ager<sup>\*ac</sup>

BiVO<sub>4</sub> thin film photoanodes were grown by vapor transport chemical deposition on FTO/glass substrates. By controlling the flow rate, the temperatures of the Bi and V sources (Bi metal and V<sub>2</sub>O<sub>5</sub> powder, respectively), and the temperature of the deposition zone in a two-zone furnace, single-phase monoclinic BiVO<sub>4</sub> thin films can be obtained. The CVD-grown films produce global AM1.5 photocurrent densities up to 1 mA cm<sup>-2</sup> in aqueous conditions in the presence of a sacrificial reagent. Front illuminated photocatalytic performance can be improved by inserting either a SnO<sub>2</sub> hole blocking layer and/or a thin, extrinsically Mo doped BiVO<sub>4</sub> layer between the FTO and the CVD-grown layer. The incident photon to current efficiency (IPCE), measured under front illumination, for BiVO<sub>4</sub> grown directly on FTO/glass is about 10% for wavelengths below 450 nm at a bias of +0.6 V vs. Ag/AgCl. For BiVO<sub>4</sub> grown on a 40 nm SnO<sub>2</sub>/20 nm Mo-doped BiVO<sub>4</sub> back contact, the IPCE is increased to over 40% at wavelengths below 420 nm.

Received 14th September 2013,  
Accepted 1st November 2013

DOI: 10.1039/c3cp53904k

www.rsc.org/pccp

## Introduction

Monoclinic bismuth vanadate, BiVO<sub>4</sub>, has attracted much interest in the field of solar water splitting as a promising photoanode.<sup>1</sup> It is stable in basic and neutral conditions and has a band gap of 2.4 eV. Notably, it has been reported<sup>2</sup> to photocatalyze oxygen evolution with an onset potential of ~0.3 V vs. RHE (~-0.9 vs. the reversible oxygen evolution potential) which makes it very attractive as a component of tandem photocathode/photoanode water splitting devices.<sup>3,4</sup> Also, the application of co-catalyst such as Co-Pi gives photocurrent onsets similar to those when a hole scavenger is used, showing that surface losses can be essentially eliminated in this material.<sup>5</sup> While initial reports on BiVO<sub>4</sub> used solution-based processes yielding nanopowders,<sup>6</sup> recent work has been focused on thin film synthesis using solution based precursors

and synthesis methods such as spin coating or bath dipping, electrodeposition, and spray pyrolysis.<sup>7-12</sup>

Chemical vapour deposition (CVD) has been used to synthesize high quality crystalline thin film materials for photoelectrochemical (PEC) applications.<sup>13</sup> One good example is high surface area 'cauliflower' shaped Fe<sub>2</sub>O<sub>3</sub> photoanodes synthesized by CVD by Grätzel *et al.* which showed a substantial increase in photoelectrochemical water oxidation compared to other Fe<sub>2</sub>O<sub>3</sub> systems reported in the literature.<sup>14</sup> Here, we show that high quality BiVO<sub>4</sub> thin films can be made by vapour transport CVD using a simple setup with low-cost precursor materials. The film morphology and stoichiometry can be controlled by the process conditions, most notably by the temperature and flow rate, and under optimal conditions, stoichiometric, dense, and continuous BiVO<sub>4</sub> thin films which are active as photoanodes can be deposited.

## Experimental

### BiVO<sub>4</sub> thin film growth

The bismuth vanadate thin film photoanodes were prepared by a home-made chemical vapour deposition system (CVD) based on thermal decomposition of bismuth and vanadium precursor sources. The deposition procedure is described in detail in the ESI;† a summary is given here. Fig. 1 is a sketch of the home-built CVD set-up consisting of an MTI tube furnace with two split temperature zones, connected to a manifold of gas supplies. The gas flow and growth pressure were controlled by

<sup>a</sup> Joint Center for Artificial Photosynthesis, 2929 7th Street, Berkeley, CA, USA. Tel: +1 510 486 6715

<sup>b</sup> École Polytechnique Fédérale de Lausanne, LMSC-SMX, Station 12, Lausanne, Switzerland. E-mail: esther.alarconllado@epfl.ch; Tel: +41 216936826

<sup>c</sup> Materials Sciences Division, Lawrence Berkeley National Laboratory, 1 Cyclotron Road, Berkeley, CA, USA. E-mail: ealarcon@lbl.gov, lechen@lbl.gov, JWager@lbl.gov; Tel: +1 510 486 6715

<sup>d</sup> Department of Electrical Engineering and Computer Sciences, University of California, Berkeley, Berkeley, California 94720, USA

† Electronic supplementary information (ESI) available: Further details on the synthesis method, characterization, and analysis of the charge separation efficiency can be found in the supplemental material. See DOI: 10.1039/c3cp53904k

‡ Equal author contribution.

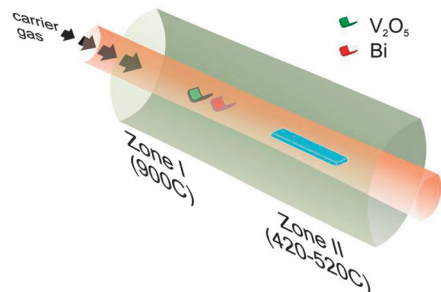


Fig. 1 Sketch of the CVD system set-up used for the growth of  $\text{BiVO}_4$  thin films.

mass flow controllers and a mechanical pump. Compressed air (99.99%) was used as the carrier gas and source of oxygen. In the two zone furnace, zone I is the high temperature zone, where the precursors, bismuth metal (Sigma Aldrich, 99.9%) and  $\text{V}_2\text{O}_5$  (Sigma Aldrich, 99.99%) powders, are evaporated. Since bismuth and  $\text{V}_2\text{O}_5$  have different melting points (271 °C and 690 °C, respectively), they were placed separately in two ceramic boats at two different locations in zone I. The mixed evaporated vapour is carried downstream by the carrier gas to zone II, where the substrate sits at a lower temperature. The temperature of the precursor zone was 900 °C while that of the deposition zone was fixed, depending on the run, at a value between 420 °C and 520 °C. The temperature was kept constant for two hours under air flow. To complete the run, the carrier gas flow was stopped and the system was allowed to reach room temperature. No post annealing of the films was employed. The substrate cleaning procedure prior to growth can be found in the ESI.† Glass coated with fluorine doped tin oxide (FTO, 25  $\Omega \text{ cm}^{-1}$ ) was used as a substrate. We also explored modifying the back contact by (1) sputtering 40 nm of  $\text{SnO}_2$  on the FTO, (2) drop casting two layers of Mo-doped  $\text{BiVO}_4$  on the FTO followed by drying at 150 °C,<sup>12</sup> forming a Mo-doped  $\text{BiVO}_4$  layer about 20 nm thick, or (3) doing (1) and (2) sequentially.

### Characterisation

The morphology and bulk elemental composition (Bi to V atomic ratio) of the films were characterized using a FEI Quanta 200 FEG scanning electron microscope (SEM) with a Bruker Quantax energy dispersive spectroscopy (EDS) attachment. Micro-Raman spectroscopy (Horiba HR-LabRam, a laser of 633 nm excitation power of 0.1–0.3 mW at the objective) and X-Ray diffraction (Rigaku Smartlab diffractometer operated at grazing angle of 1°) were used to assess the crystal structure and the presence/absence of V rich or Bi rich secondary phases. The optical absorbance spectrum was measured by a Shimadzu SolidSpec-3700 UV-Vis-NIR Spectrophotometer.

A SolarLight 16S-300-005 solar simulator equipped with an AM1.5 filter set was used as light source for photoelectrochemical (PEC) characterisation and the light intensity was adjusted to 100  $\text{mW cm}^{-2}$ . Electrochemical analysis was performed with a Biologic SP-300 potentiostat in an aqueous pH 7  $\text{K}_2\text{HPO}_4$  buffer solution with 0.5 M  $\text{Na}_2\text{SO}_3$  serving as a sacrificial reagent. For the incident photon to current efficiency

(IPCE) measurements, a 150 W Xe lamp (Newport) coupled to an Oriel Cornerstone 1/8m monochromator with 1.5 mm slits was used. A Thorlabs FDS1010-CAL calibrated Si photodiode was used to calibrate the flux of photons impinging on the sample. Potential and current were controlled through a Gamry Reference 600 potentiostat.

## Results and discussion

### Deposition conditions and structural characterisation

The primary challenge in the CVD deposition of bismuth vanadate is obtaining the desired phase in a narrow range of Bi and V chemical potentials while avoiding secondary phases.<sup>15,16</sup> The theoretical synthesis phase diagram of Yin *et al.*<sup>15</sup> was used as a guide in this work. We found an interplay between the temperature in the deposition zone (zone II) and the flow rate. The substrate temperature range we explored was from 420 °C to 500 °C. We found that the higher the growth temperature, the larger the air flow was required to obtain films with similar atomic composition. Similarly, when lower temperatures were used, the gas flow needed to be reduced for obtaining stoichiometric monoclinic  $\text{BiVO}_4$ . In the following discussion, we discuss in more detail about the influence of the synthesis parameters of zone II temperatures and flow rates respectively, by varying one parameter while setting the other constant.

### The influence of air flow rate

Fig. 2(a–c) shows the SEM images of a few representative films obtained by varying the carrier gas flow rate (100 sccm, 200 sccm and 300 sccm) at a deposition zone temperature of 460 °C.

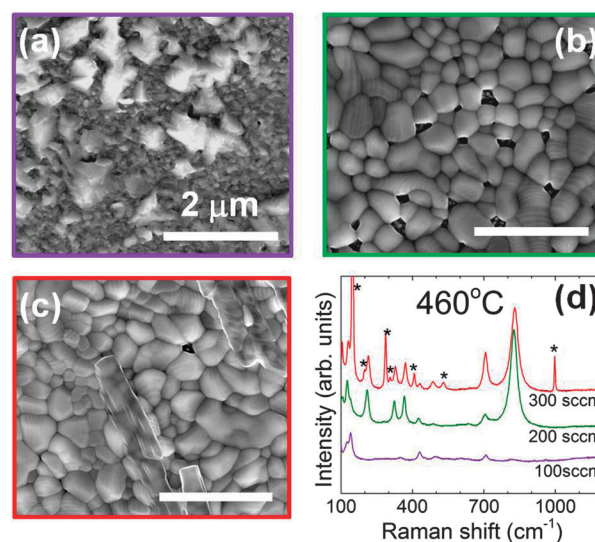


Fig. 2 SEM images of CVD deposited films at 460 °C zone II temperature and under a gas flow of (a) 100, (b) 200 and (c) 300 sccm. The Raman spectra of the films are shown in (d). While at a flow of 100 sccm, no  $\text{BiVO}_4$  is formed, at a flow of 300 sccm, there is the presence of secondary  $\text{V}_2\text{O}_5$  phase, reflected by wire structures in (c) and in the Raman spectrum in (d), marked by \*. A flow of 200 sccm produces a stoichiometric film without the  $\text{V}_2\text{O}_5$  impurity phase.

The growth time was the same for all samples. As one could expect, the film coverage increases with flow rate, since it enables a faster growth rate. At a low flow rate (100 sccm, Fig. 2(a)), no bismuth vanadate is obtained and only  $\text{Bi}_2\text{O}_3$  crystals were formed for lower fluxes (not shown), while at high flow (300 sccm) we see evidence of a secondary phase of vanadium oxide in the form of 1-D wire/rod structures (Fig. 2(c), V:Bi > 60:40 according to EDS analysis). Stoichiometric  $\text{BiVO}_4$  is obtained at an intermediate flow rate of 200 sccm (Fig. 2(b)). Both of  $\text{BiVO}_4$  thin film part in Fig. 2(b) and (c), have a smooth and continuous polycrystalline structure with similar grain size of about a few hundreds of nanometers in diameter.

Fig. 2(d) contains the Raman spectra of three CVD grown  $\text{BiVO}_4$  thin films under different flow rates at a fixed zone II temperature of 460 °C. The spectrum of the sample grown under 200 sccm is that of monoclinic  $\text{BiVO}_4$  (see ESI† for a more detailed description of phase identification by Raman spectroscopy). The most prominent Raman feature of monoclinic  $\text{BiVO}_4$  is centred at around  $827\text{ cm}^{-1}$  and corresponds to a stretching symmetric V–O mode. Then, a doublet at 326 and  $367\text{ cm}^{-1}$  correspond to deformation of  $\text{VO}_4$  tetrahedra, while a band around 211 and  $129\text{ cm}^{-1}$  are lattice modes. Highly crystalline pure stoichiometric and monoclinic  $\text{BiVO}_4$  was obtained for flow rate of 200 sccm. On the other hand, the presence of different bismuth oxide polymorphs-related vibrational modes was weakly observed if the growth was performed under low flow rates (100 sccm and below-not shown), while  $\text{V}_2\text{O}_5$ -related vibrational peaks were clearly detected for the samples grown under high flow rates (300 sccm and higher).

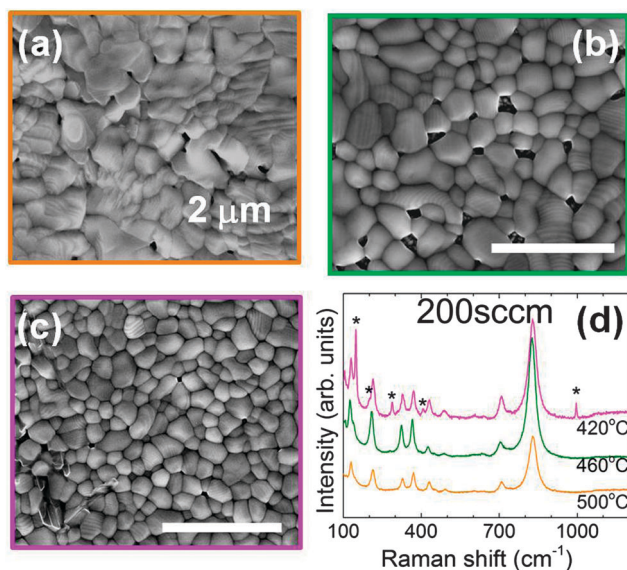


Fig. 3 Raman spectrum of CVD-grown  $\text{BiVO}_4$  thin films grown under 200 sccm flow rate and at (a) 500, (b) 460 and (c) 420 °C. Raman spectra of the same films are shown in (d). Again, the secondary  $\text{V}_2\text{O}_5$  phase appears in the Raman spectrum of the film grown at the lowest temperature ( $\text{V}_2\text{O}_5$  Raman features marked with \*).

## The influence of zone II temperature

We found that the substrate temperature (zone II) provided fine tuning of the Bi to V stoichiometry. Fig. 3(a) to (c) show the SEM images of three  $\text{BiVO}_4$  films deposited at different zone II temperature of 500 °C, 460 °C and 420 °C at a flow rate of 200 sccm, respectively. V rich  $\text{BiVO}_4$  (V:Bi  $\sim$  56:44) was obtained when grown at lower temperature (420 °C) with trace phase segregation of vanadium oxide. Contrarily, the highest temperature (500 °C) conditions shown here produced a slightly Bi rich film (V:Bi  $\sim$  48:52). Finally,  $\text{BiVO}_4$  with V:Bi  $\sim$  52:48 was obtained at 460 °C substrate temperature. Compared to the latter, the vanadium-rich film has smaller but denser crystals and the Bi rich film shows more layered and a rougher structure.

Fig. 3(d) shows the Raman spectra for  $\text{BiVO}_4$  films grown at different zone II temperatures. As discussed below, we found the highest photoanodic response, and thus probably the highest n-type conductivity, for thin films grown at a substrate temperature of 460 °C, for which the Raman spectrum matches that of monoclinic  $\text{BiVO}_4$ . At lower temperatures (420 °C), the vanadium oxide phase appears while at higher temperatures ( $\sim$  500 °C) the monoclinic  $\text{BiVO}_4$  Raman peaks significantly decrease in intensity. Although Raman spectroscopy is very sensitive for detecting certain secondary phases, it is less sensitive to the formation of Bi rich Bi–V–O binary oxide compounds. XRD on the other hand, is able to identify distinct spectra from the formation of these Bi rich compounds. Fig. 4 shows XRD spectra of two samples deposited at 500 °C and 460 °C. In addition to the formation of monoclinic  $\text{BiVO}_4$  as shown in Fig. 4(b), the Bi-rich sample also shows the co-existence of  $\text{Bi}_2\text{VO}_{5.5}$  (assigned in the figure).

## The influence of underlayers

Several strategies have been reported in the literature in order to improve the PEC performance of  $\text{BiVO}_4$  films, including doping with Mo or W to improve conductivity,<sup>4,12,17,18,20</sup> and using hole blocking layers next to the back contact.<sup>4,7</sup> Here we explored different substrate underlayers for improving the photo-anodic performance of our CVD-grown films. For this purpose,  $\text{BiVO}_4$  films were grown under the optimum temperature and flow conditions found in the previous section (460 °C and

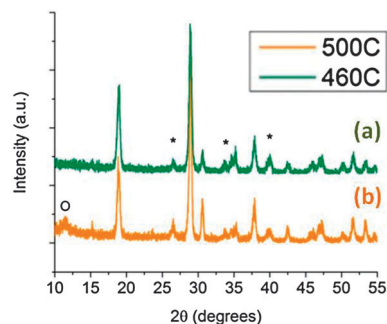


Fig. 4 X-ray diffraction pattern of (a) stoichiometric (deposited at 460 °C) and (b) slightly Bi rich (deposited at 500 °C) thin films. The “\*” labelled peaks are coming from FTO substrate and “o” labelled peak is assigned to the (002) reflection of  $\text{Bi}_2\text{VO}_{5.5}$ .

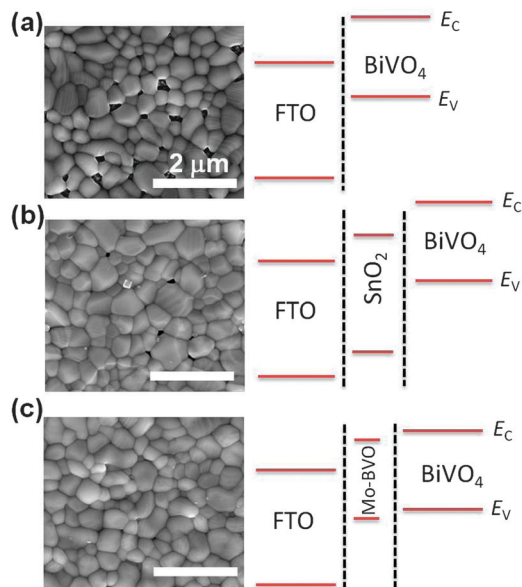


Fig. 5 SEM images of CVD deposited films at 460 °C zone II temperature and under 200 sccm air flow (7.7 Torr total pressure), on (a) FTO, (b) SnO<sub>2</sub>/FTO and (c) on Mo-BiVO<sub>4</sub> precursor coated FTO. On the right, a schematic band alignment is shown (charge redistribution is not considered).

200 sccm, respectively) on (1) plain FTO, (2) two layers of Mo-doped BiVO<sub>4</sub> drop casted uniformly on FTO, (3) 40 nm sputtered SnO<sub>2</sub> on FTO, and (4) a combination of 2 and 3.

We first address the morphology of the as-grown films on top of the different substrate configurations. Fig. 5 shows the SEM image of the CVD-grown BiVO<sub>4</sub> on FTO, SnO<sub>2</sub>/FTO and Mo-doped BiVO<sub>4</sub>/FTO. Next to the SEM pictures, a schematic representation of the structure band alignment is given for the three configurations considered in the figure. As discussed in detail in the ESI,<sup>†</sup> the pre-treatment of the substrate surface previous to CVD-growth can affect the coverage of BiVO<sub>4</sub> films. As well, we found that the presence of underlayers like SnO<sub>2</sub> and Mo-doped BiVO<sub>4</sub> can further improve the film coverage. It appears that thin SnO<sub>2</sub> and Mo-doped BiVO<sub>4</sub> coatings serve as seeding layers to promote the growth of BiVO<sub>4</sub> crystals in the CVD reactor. The overall coverage of BiVO<sub>4</sub> on different underlayers is in the order of Mo:BiVO<sub>4</sub>/FTO > SnO<sub>2</sub>/FTO > FTO. In the case of the CVD film grown on Mo:BiVO<sub>4</sub>/FTO (depicted in Fig. 5(c)), a full coverage is indicated by the absence of Mo at the surface of the film according to XPS measurements, as shown in Fig. S4 in the ESI.<sup>†</sup> Finally, the morphology of the film deposited on Mo:BiVO<sub>4</sub>/SnO<sub>2</sub>/FTO was very similar to the one on Mo:BiVO<sub>4</sub>/FTO and thus is not shown here (see ESI,<sup>†</sup> Fig. S2). Other than coverage, the different underlayers do not seem to affect the final film composition and grain morphology, including crystal size and shape. All the deposited BiVO<sub>4</sub> films display a smooth grain structure with a relatively large grain size from a couple hundreds of nanometers to almost one micron in diameter.

### Photo-electrochemical characterisation

Photoelectrochemical measurements were performed for CVD-grown films of similar thickness, ~200 nm. The photoelectrochemical performance of BiVO<sub>4</sub> films grown at different

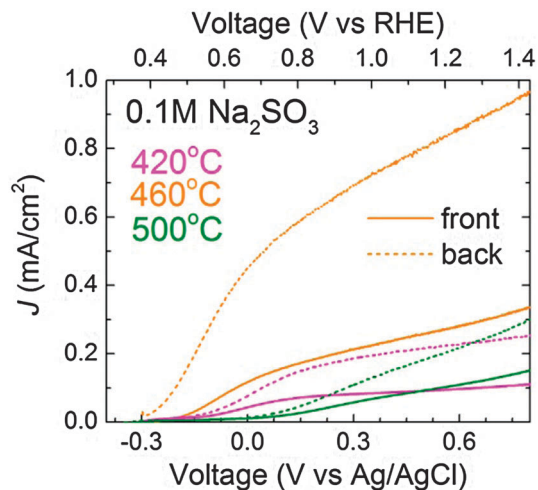


Fig. 6 Linear sweep voltammetry on illuminated BiVO<sub>4</sub> films grown on FTO/glass substrate at different zone II temperatures. Measurements were performed at pH 7 with NaSO<sub>3</sub> as a sacrificial reagent. Front/back illuminated curves are represented by solid/dashed lines.

temperatures is shown in Fig. 6. All electrochemical tests were performed in the presence of a sacrificial hole acceptor for overcoming the slow oxidation kinetics at the BiVO<sub>4</sub> surface. As reported previously in the BiVO<sub>4</sub> literature, we observe a higher photocurrent with illumination through the transparent substrate (back illumination) as compared to front illuminated films in all our bare CVD-grown BiVO<sub>4</sub> samples.<sup>9</sup> The difference was strongly reduced with film thickness, becoming quite negligible for films around 100 nm thick (see ESI,<sup>†</sup> Fig. S5(b)). This result is consistent with the hypothesis of Liang *et al.* of poor electron transport in BiVO<sub>4</sub>.<sup>7</sup>

As mentioned earlier, samples grown at 460 °C under 200 sccm air flow gave the highest photoelectrochemical response. Also, as mentioned above, this film appears to have a slight excess of V according to the EDS analysis. On the other hand, the Bi-rich BiVO<sub>4</sub> film exhibits a decreased onset potential as well as reduced photocurrent, which is consistent with our recent study of the effects of stoichiometry on the performance of sputtered BiVO<sub>4</sub> films.<sup>19</sup> We attribute this result to a superior electron conductivity obtained by tuning to slight V-rich conditions, which encourages the formation of V interstitials ( $V_{\text{int}}$ ) and V antisites ( $V_{\text{Bi}}$ ), while discouraging Bi vacancies ( $\text{Bi}_v$ ). Such defects are in fact predicted to be donors and compensating acceptors, respectively.<sup>15</sup> Our best performing BiVO<sub>4</sub> films grown directly on FTO/glass show similar or lower front-illuminated photocurrent as compared to some undoped BiVO<sub>4</sub> photoanodes found in the literature measured under similar test conditions.<sup>20</sup> One contributing factor to our relatively low photocurrent is that our films are highly reflective (30–40% for the 300–600 nm spectral range, Fig. S8a, ESI<sup>†</sup>), which will result into significantly reduced photocurrents as compared to those from textured films. Also, we must mention that a similar photoresponse was obtained with films grown on indium tin oxide, or ITO, on glass substrates instead of FTO (see ESI,<sup>†</sup> Fig. S5(a)).

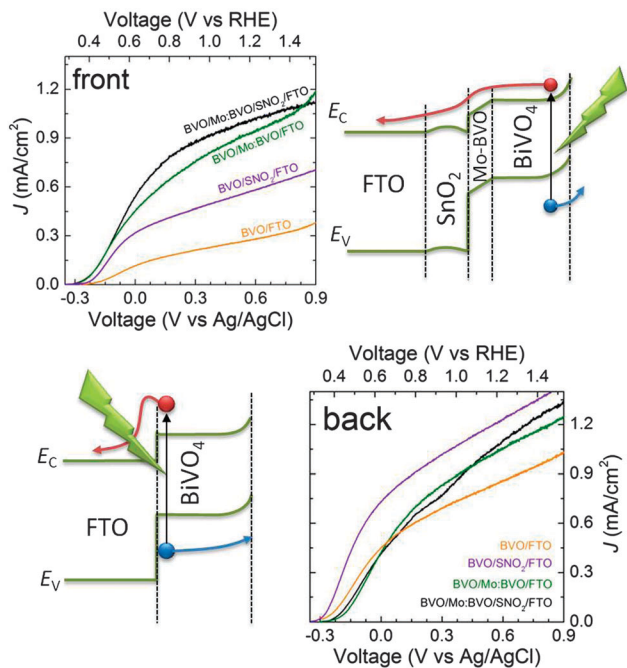


Fig. 7 (top) Linear sweep voltammetry on front illuminated CVD-grown  $\text{BiVO}_4$  thin films with different substrate underlayers. Also, the diagram illustrating the path for carriers photo-generated at the surface of the photoanode on  $\text{Mo-BiVO}_4/\text{SnO}_2/\text{FTO}$  substrate is shown. (bottom) Linear sweep voltammetry on the same samples illuminated from the back side. Now, the diagram is shown for carriers generated close to the interface with the back contact in the case of  $\text{BiVO}_4$  grown directly on FTO substrate.

On the other hand, the use of substrate underlayers has a large effect on the PEC performance of CVD-grown  $\text{BiVO}_4$  films. Linear sweep voltammograms, with either front or back illumination, as a function of the different substrate underlayers are shown in Fig. 7. One can first observe that the effects of the presence of underlayers are much larger in the case of front illumination as compared to back-illumination. Front-illuminated photocurrent of a CVD-grown  $\text{BiVO}_4$  film is almost doubled (from  $0.28$  to  $0.58 \text{ mA cm}^{-2}$  @  $1.23 \text{ V vs. RHE}$ ) by the addition of a thin sputtered  $\text{SnO}_2$  interlayer and more than tripled (from  $0.28$  to  $0.95 \text{ mA cm}^{-2}$  @  $1.23 \text{ V vs. RHE}$ ) by just inserting a drop casted  $20 \text{ nm}$ -layer of Mo-doped  $\text{BiVO}_4$  on top of FTO. As also shown in Fig. 7, the underlayer treatments also increase the photocurrent under back illumination, but to a smaller extent.

We discuss first the effect of the  $\text{SnO}_2$  underlayer. In addition to the idea that a  $\text{SnO}_2$  layer on a FTO substrate acts as a “hole mirror” due to its highly positive valence band edge, it has also suggested that the use of a  $\text{SnO}_2$  layer reduces the concentration of interface states at the back contact.<sup>7,9</sup> Defects at the  $\text{BiVO}_4/\text{FTO}$  interface can act as recombination centres, which can trap free photo-generated electrons and thus reducing the total photocurrent. Also, the negatively charged bound electrons at the interface can act as a rather effective recombination centres for photo-holes that are generated close to the interface or that have reached the interface by diffusion.

This explains why bare  $\text{BiVO}_4$  on FTO shows the lowest back-illuminated photocurrent of all samples in this work. By incorporating a  $\text{SnO}_2$  layer on top on FTO substrate, we may be partially filling such interface states as well as preventing holes that are close to the back contact to recombine with trapped electrons. A similar effect may be operating with the Mo-doped  $\text{BiVO}_4$  underlayer. In this case, the band alignment with FTO is similar, however electrons from the Mo-doped layer can fill the interface states at the FTO surface, which reduces not only recombination at the back contact but also the presence of possible unfavourable band bending. Interestingly, we observe that the addition of  $\text{SnO}_2$  in between Mo-doped  $\text{BiVO}_4$  and FTO leads to only a small additional increase in photocurrent, which corroborates that most of the current enhancement is due to interface state filling.

The photocurrent can be expressed as the product of the catalytic efficiency  $\eta_{\text{cat}}$ , charge separation efficiency  $\eta_{\text{sep}}$ , and carrier generation rate produced by photon absorption.<sup>21</sup> Since a strong oxidizer was used as a sacrificial reagent for measuring the PEC performance, we can assume that the catalytic efficiency  $\eta_{\text{cat}}$  is close to 1. Also, the samples we evaluated had showed very similar Bi:V composition, morphology and absorption coefficients (see previous sections and inset in Fig. 8). As a result, the photocurrent enhancement must be mostly due to an improved separation efficiency of the photo-generated electron-hole pairs ( $\eta_{\text{sep,1sun}}$ ). Following a similar approach as in ref. 4 and 21 (see ESI† for details), we calculate  $\eta_{\text{sep,1sun}}$  for the films shown in Fig. 7. At  $1.2 \text{ eV vs. RHE}$ , we obtain the  $\eta_{\text{sep}}$  values of 10.6, 22, 35.7 and 38.4% for  $\text{BiVO}_4$  films grown on FTO,  $\text{SnO}_2/\text{FTO}$ ,  $\text{Mo:BiVO}_4/\text{FTO}$  and  $\text{Mo:BiVO}_4/\text{SnO}_2/\text{FTO}$ , respectively (see Table 1). While further improvements in separation efficiency are clearly desirable, we note that our highest values are comparable to prior

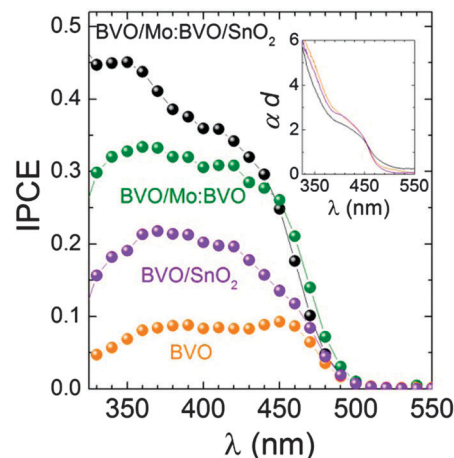


Fig. 8 Incident photon to current conversion efficiency for front-illuminated CVD-grown  $\text{BiVO}_4$  thin films at  $0.6 \text{ V vs. Ag/AgCl}$  ( $1.21 \text{ V vs. RHE}$ ) as a function of wavelength. The presence of an initial layer of Mo-doped casted  $\text{BiVO}_4$  improves the photo-carrier extraction efficiency for the overall absorption spectral range. Inset: absorbance as a function of wavelength of the films used in the PEC experiments. It can be seen that the total absorbed light is very similar for all films, regardless of the underlayer.

**Table 1** Electron–hole separation efficiency (see text) for CVD-grown BiVO<sub>4</sub> films grown with the indicated back contacts

Sample configuration	$\eta_{\text{sep}}$ (1 sun)%	$\eta_{\text{sep},\lambda}$ (360 nm)%	$\eta_{\text{sep},\lambda}$ (450 nm)%
BiVO <sub>4</sub> /FTO	10.6	12	19
BiVO <sub>4</sub> /SnO <sub>2</sub> /FTO	22.0	33	28
BiVO <sub>4</sub> /Mo-BiVO <sub>4</sub> /FTO	35.7	50	50
BiVO <sub>4</sub> /Mo-BiVO <sub>4</sub> /SnO <sub>2</sub> /FTO	38.4	68	51

literature reports, *e.g.* W-doped BiVO<sub>4</sub> films ( $\sim 40\%$  at 1.23 V vs. RHE).<sup>4</sup>

In order to further assess the photo-anodic performance of the CVD-grown BiVO<sub>4</sub> films and effects of the underlayers, we show the incident to photon conversion efficiency, IPCE (or EQE) as a function of incident wavelength under front-illumination conditions (Fig. 8). The experiments were also performed with the presence of a sacrificial reagent at +0.6 V vs. Ag/AgCl. As expected from the photo-current response, the IPCE is increased when a SnO<sub>2</sub> and/or Mo-doped BiVO<sub>4</sub> layers are present at the interface with the FTO substrate. The overall shape of the efficiency curve is similar for all samples, rising steeply at a wavelength of around 500 nm, in accordance to the measured absorbance (inset Fig. 8) and to previous works.<sup>4,7,19,20</sup> Analogously to the charge separation efficiency analysis extracted from the photocurrent, one can also consider the IPCE as a product of absorption, catalytic and charge separation efficiencies, thus leaving the IPCE improvement mostly a function of charge carrier separation efficiency. We consider two representative wavelengths, 360 nm and 450 nm. The charge separation efficiency for the specified wavelengths is calculated from the IPCE, absorption and reflectance as described in the ESI† (Fig. S9 and S10).

A summary of the charge separation efficiencies for samples with different substrate underlayers is provided in Table 1. As expected, the separation efficiency is improved over the whole wavelength range. Interestingly, the improvement produced by the underlayers is more prominent for wavelengths smaller than 400 nm, for which carriers are mostly absorbed within the top  $\sim 80$  nm. This is in agreement with the front *versus* back-illuminated *JV* curves, where the underlayers produce the biggest effect on the front-illuminated photocurrent. It is interesting that modifying the back contact has the largest effect on charge carriers created near the film/electrolyte interface. As we are not actually modifying the bulk properties of the material by the incorporation of extra layers on top of the FTO substrate, we believe that the underlayers can fill interface states and/or reduce a possible Schottky barrier between BiVO<sub>4</sub> and FTO, as shown schematically in Fig. 7. This apparently increases the efficiency of collecting electrons created far away from the back contact.

## Conclusions

We demonstrate for the first time, the chemical vapour transport growth of high quality, crystalline monoclinic bismuth

vanadate films from solid precursors. We are able to control both film stoichiometry and morphology with the growth conditions of air flow rates and deposition zone temperatures. High air flow rate and deposition zone temperature facilitates the growth of vanadium rich phases. Low air flow rate and deposition zone temperature facilitates the growth of bismuth rich phases. Under optimum conditions, stoichiometric films of monoclinic BiVO<sub>4</sub> without observable secondary phases are produced. We note that the stoichiometry control afforded by the technique could allow, for example, for gradient doping by adjusting the air flow during growth.

The effect of different underlayers applied prior to the CVD growth was investigated. The improvements in photocurrent were larger for front illumination compared to back. For films grown under optimal conditions, the use of either a thin Mo-doped BiVO<sub>4</sub> layer or this layer combined with a SnO<sub>2</sub> underlayer produced the best performance. One sun charge separation efficiency  $\sim 38\%$  and peak wavelength efficiencies over 60% were produced in the presence of sacrificial reagents.

## Acknowledgements

This material is based upon work performed by the Joint Center for Artificial Photosynthesis, a DOE Energy Innovation Hub, supported through the Office of Science of the U.S. Department of Energy under Award Number DE-SC0004993. EAL acknowledges fellowship support from Marie Curie Actions Program.

## Notes and references

- 1 Y. Park, K. J. McDonald and K.-S. Choi, *Chem. Soc. Rev.*, 2013, **42**, 2321.
- 2 D. K. Zhong, S. Choi and D. R. Gamelin, *J. Am. Chem. Soc.*, 2011, **133**, 18370.
- 3 Q. Jia, K. Iwashina and A. Kudo, *Proc. Natl. Acad. Sci. U. S. A.*, 2012, **109**, 11564.
- 4 F. Abdi, L. Han, A. H. M. Smets, M. Zeman, B. Dam and R. van de Krol, *Nat. Commun.*, 2013, **4**, 2195.
- 5 K. Sivula, *J. Phys. Chem. Lett.*, 2013, **4**, 1624.
- 6 A. Kudo, K. Omori and H. Kato, *J. Am. Chem. Soc.*, 1999, **121**, 11459.
- 7 Y. Liang, T. Tsubota, L. P. A. Mooij and R. van de Krol, *J. Phys. Chem. C*, 2011, **115**, 17594.
- 8 J. Su, L. Guo, N. Bao and C. A. Grimes, *Nano Lett.*, 2011, **11**, 1928.
- 9 F. F. Abdi and R. van de Krol, *J. Phys. Chem. C*, 2012, **116**, 9398.
- 10 J. A. Seabold and K.-S. Choi, *J. Am. Chem. Soc.*, 2012, **134**, 2186.
- 11 R. Saito, Y. Miseki and K. Sayama, *Chem. Commun.*, 2012, **48**, 3833.
- 12 W. Luo, Z. Yang, Z. Li, J. Zhang, J. Liu, Z. Zhao, Z. Wang, S. Yan, T. Yu and Z. Zou, *Energy Environ. Sci.*, 2011, **4**, 4046.
- 13 J. Shi, Y. Hara, C. Sun, M. A. Anderson and X. Wang, *Nano Lett.*, 2011, **11**, 3413.

- 14 A. Kay, I. Cesar and M. Grätzel, *J. Am. Chem. Soc.*, 2006, **49**, 15714.
- 15 W.-J. Yin, S.-H. Wei, M. M. Al-Jassim, J. Turner and Y. Yan, *Phys. Rev. B: Condens. Matter Mater. Phys.*, 2011, **83**, 155102.
- 16 G. Wang, Y. Ling, X. Lu, F. Qian, Y. Tong, J. Z. Zhang, V. Lordi, C. R. Leao and Y. Li, *J. Phys. Chem. C*, 2013, **117**, 10957.
- 17 W. Luo, Z. Li, T. Yu and Z. Zou, *J. Phys. Chem. C*, 2012, **116**, 5076.
- 18 H. W. Jeong, T. H. Jeon, J. S. Jang, W. Choi and H. Park, *J. Phys. Chem. C*, 2013, **117**, 9104.
- 19 L. Chen, E. Alarcon-Llado, M. Hettick, I. D. Sharp, Y. Lin, A. Javey and J. W. Ager, *J. Phys. Chem. C*, DOI: 10.1021/jp406019r.
- 20 S. P. Berglund, A. J. E. Rettie, S. Hoang and C. B. Mullins, *Phys. Chem. Chem. Phys.*, 2012, **14**, 70.
- 21 H. Dotan, K. Sivula, M. Graetzel, A. Rothschild and S. C. Warren, *Energy Environ. Sci.*, 2011, **4**, 958.